Electron recombination with multicharged ions via chaotic many-electron states

V. V. Flambaum,[1] A. A. Gribakina,[1,*] G. F. Gribakin,[2] and C. Harabati[1]
[1]*School of Physics, The University of New South Wales, Sydney, UNSW 2052, Australia*
[2]*Department of Applied Mathematics and Theoretical Physics, Queen's University, Belfast BT7 1NN, United Kingdom*
(Received 7 June 2001; revised manuscript received 4 January 2002; published 22 July 2002)

We show that a dense spectrum of chaotic multiply excited eigenstates can play a major role in collision processes involving many-electron multicharged ions. A statistical theory based on chaotic properties of the eigenstates enables one to obtain relevant energy-averaged cross sections in terms of sums over single-electron orbitals. Our calculation of low-energy electron recombination of Au^{25+} shows that the resonant process is 200 times more intense than direct radiative recombination, which explains the recent experimental results of Hoffknecht *et al.* [J. Phys. B **31**, 2415 (1998)].

DOI: 10.1103/PhysRevA.66.012713 PACS number(s): 34.80.Lx, 31.10.+z, 32.80.Dz, 34.10.+x

I. INTRODUCTION

In this paper we give a quantitative explanation of the puzzle of electron recombination with Au^{25+}. We also demonstrate how to calculate the contribution of ''chaotic'' multiply excited states of the compound ion, which mediate electron recombination with complex many-electron ions.

Experimentally, this process was studied recently at the UNILAC heavy ion accelerator facility of the GSI in Darmstadt [1]. In spite of a high energy resolution [2] the measured recombination rate did not reveal any resonances and only showed two broad structures around 30 and 80 eV. However, its magnitude at low electron energies $\varepsilon \sim 1$ eV exceeded the radiative recombination (RR) rate by two orders of magnitude [3], although the observed energy dependence was close to that of RR.

It is well known that recombination rates are often enhanced by dielectronic recombination (DR). In this process the incident electron is captured in a doubly excited state of the compound ion, which is then stabilized by photoemission. Suggested originally by Sayers, it was first considered by Massey and Bates [4] in the problem of ionospheric oxygen. Later, DR was found to be important for the ionization balance in the solar corona and high-temperature plasmas in general [5]. Electron-ion recombination has been measured directly in the laboratory since the early 1980s [6]. More recently, the use of heavy-ion accelerators and electron coolers of ion storage rings has greatly advanced the experiments [7,8]. Recombination rates for many ions have been measured at electron energies from threshold to hundreds of electron volts with resolution of a fraction of an eV [9–15]. For few-electron ions the measured rates were in good agreement with theory, which included the contribution of DR resonances on top of the RR background, e.g., in He^+ [16], Li-like C^{4+} [15] and Ar^{15+} [9,14], and B-like Ar^{13+} [17]. However, more complicated ions, e.g., Au^{50+} [13] and U^{28+} [12], showed complicated resonance spectra and strongly enhanced recombination rates at low electron energies. In particular, in U^{28+} the theory was able to explain the main resonant features in the range 80–180 eV, but failed to identify the resonances and reproduce the rate at smaller energies [18]. The situation in Au^{25+} [1] looks even more puzzling.

II. MANY-ELECTRON EXCITATIONS

In Ref. [19] we suggested that electron recombination with Au^{25+} is mediated by complex *multiply excited* states of Au^{24+}, rather than ''simple'' dielectronic resonances. Electrons could be captured in these states due to a strong configuration interaction in this open-shell system. The ground state of Au^{24+} is described by the $1s^2 \ldots 4d^{10}4f^9$ configuration. Figure 1 shows the spectrum of relativistic single-particle orbitals of Au^{24+}. The occupied orbitals (below the Fermi level) are found in a relativistic Dirac-Fock calculation of the Au^{24+} ground state, and the excited state orbitals (above the Fermi level) are obtained by solving the Dirac-Fock equation for an electron in the potential of Au^{25+} $1s^2 \ldots 4f^8$.

The single-particle spectrum of Au^{24+} does not have large gaps. Using the single-particle orbitals we have generated many-electron configurations, evaluated their energies, and estimated the energy density of multiply excited states [19]. Owing to the ''gapless'' single-particle spectrum, the density

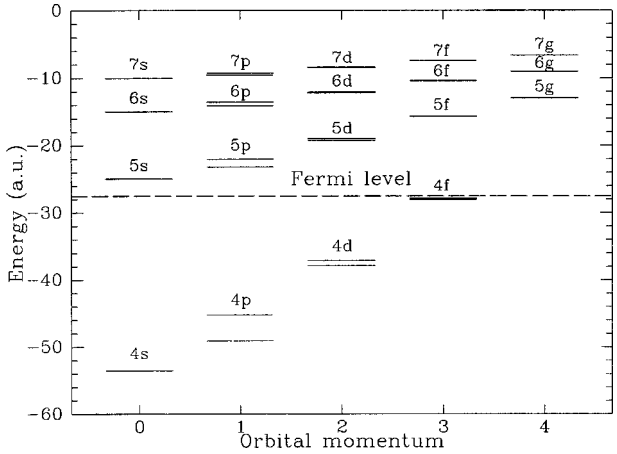

FIG. 1. Energies of occupied and vacant single-particle orbitals of Au^{24+} obtained in a Dirac-Fock calculation.

*Present address: East Antrim Institute of Further and Higher Education, Newtownabbey BT37 9RS, Northern Ireland.

increases rapidly as a function of energy, as described by the Fermi-gas-model ansatz [20],

$$\rho(E)=AE^{-\nu}\exp(a\sqrt{E}), \tag{1}$$

with $A=31.6$, $\nu=1.56$, and $a=3.35$ a.u. [21], where E is the energy above the ground state in atomic units, which we use throughout the paper.

Ionic eigenstates are characterized by their total angular momentum and parity J^π, and are $2J+1$ times degenerate. Therefore the total level density can be broken into a sum of partial level densities: $\rho(E)=\Sigma_{J\pi}(2J+1)\rho_{J\pi}(E)$. The excitation spectrum of Au^{24+} near the ionization threshold $E=I\approx 27.5$ a.u. contains many J ranging from $\frac{1}{2}$ to $\frac{35}{2}$ [19]. Their distribution is in agreement with statistical theory [20,22], which predicts that at a given energy $\rho_{J\pi}$ are proportional to the function

$$f(J)=\frac{2(2J+1)}{(2J_m+1)^2}\exp\left[-\frac{(2J+1)^2}{2(2J_m+1)^2}\right], \tag{2}$$

where J_m is the most abundant J value. Numerically for Au^{24+} we find $J_m\approx\frac{9}{2}$.

Using Eq. (2) one can estimate the partial densities by $\rho_J=\rho_{J^+}+\rho_{J^-}\simeq f(J)\rho/\langle 2J+1\rangle$, where $\langle 2J+1\rangle$ is an average over $f(J)$ [23]. For the most abundant angular momenta $J\sim J_m$, and assuming $\rho_{J^+}\approx\rho_{J^-}$, we have $\rho_{J\pi}(E)=A_{J\pi}E^{-\nu}\exp(a\sqrt{E})$ with $A_{J\pi}\approx 0.15$. Near the ionization threshold this gives $\rho_{J\pi}\approx 3.6\times 10^4$ a.u., which means that the spacing between the multiply excited states with a given J^π is very small: $D=1/\rho_{J\pi}\sim 1$ meV. This would explain why individual autoionizing resonances in electron recombination on Au^{25+} could not be resolved experimentally [19]. However, the large density of multiply excited states is only a ''kinematic'' reason behind the experimental observation, because we have not yet proved that the electron can actually be captured in these states. In what follows we analyze the dynamics of electron capture and show that the residual Coulomb interaction between the electrons (i.e., that beyond the mean field) makes for an efficient capture and accounts for the observed enhanced recombination rate.

Taking into account this interaction is the key problem in many-electron processes. In general, this can be achieved by constructing a basis of many-electron states Φ_k from single-particle (e.g., Dirac-Fock) orbitals, and solving the eigenproblem for the Hamiltonian matrix $H_{ik}=\langle\Phi_i|\hat{H}|\Phi_k\rangle$, which yields the eigenvalues E_ν and eigenstates $|\Psi_\nu\rangle=\Sigma_k C_k^{(\nu)}|\Phi_k\rangle$ of the system (configuration interaction method). For open-shell systems with a few valence electrons, e.g., rare-earth atoms, this becomes an increasingly difficult task. The density of states grows very rapidly with the excitation energy, and finding the eigenstates requires diagonalization of ever greater matrices.

On the other hand, when the level density is high and the two-body interaction is sufficiently strong the system is driven into a regime of *many-body quantum chaos*, where the effect of configuration mixing can be described statistically. This regime is characterized by the following [24,25]. (i) Each eigenstate contains a large number N of *principal* components $C_k^{(\nu)}\sim 1/\sqrt{N}$, corresponding to the basis states Φ_k which are strongly mixed together. (ii) Owing to the strong mixing, the only good quantum numbers that can be used to classify the eigenstates, are the exactly conserved total angular momentum and parity J^π and the energy. (iii) The degree of mixing in this regime is in some sense complete, i.e., all basis states that can be mixed (within a certain energy range; see below) are mixed. The notion of configurations based on the single-particle orbitals becomes largely irrelevant for the purpose of classifying the eigenstates. Each eigenstate contains substantial contributions of a few nearby configurations.

This strong mixing takes place in a certain energy range $|E_k-E_\nu|\lesssim\Gamma_{\rm spr}$, where $E_k\equiv H_{kk}$ is the mean energy of the basis state and $\Gamma_{\rm spr}$ is the so-called *spreading width*. More precisely, the mean-squared value of $C_k^{(\nu)}$ as a function of E_k-E_ν, can be described by a Breit-Wigner formula

$$\overline{|C_k^{(\nu)}|^2}=N^{-1}\frac{\Gamma_{\rm spr}^2/4}{(E_k-E_\nu)^2+\Gamma_{\rm spr}^2/4}, \tag{3}$$

with $N=\pi\Gamma_{\rm spr}/2D$ fixed by the normalization $\Sigma_k|C_k^{(\nu)}|^2\simeq\int\overline{|C_k^{(\nu)}|^2}dE_k/D=1$. The decrease of $C_k^{(\nu)}$ for $|E_k-E_\nu|>\Gamma_{\rm spr}$ is a manifestation of perturbation theory: the admixture of distant basis states is suppressed by large energy denominators. Apart from this systematic variation, the components $C_k^{(\nu)}$ behave as Gaussian random variables.

This picture of many-body quantum chaos is supported by numerical studies of nuclei [24], complex heavy atoms [25], and ions [19]. In particular, in Ref. [19] we performed a limited study of configuration mixing in Au^{24+} by diagonalizing the Hamiltonian matrix for two out of many configurations close the ionization threshold, namely, $4f_{5/2}^3 4f_{7/2}^3 5p_{1/2}5p_{3/2}5g_{7/2}$ and $4f_{5/2}^3 4f_{7/2}^3 5p_{1/2}5d_{3/2}5f_{7/2}$ [26]. These two configurations alone produce a total of 143 360 many-electron states with J between $\frac{1}{2}$ and $17\frac{1}{2}$. Even for a given J the size of the Hamiltonian matrix is large, e.g., there are 1254 states with $J^+=\frac{13}{2}^+$ (neglecting the $2J+1$ degeneracy). This calculation has shown that the configuration mixing in this system is essentially complete, since the weight of each configuration in every eigenstate is close to 50%. We have also obtained a value for the spreading width in Au^{24+}, $\Gamma_{\rm spr}\approx 0.5$ a.u., which allows one to estimate that a typical eigenstate near the ionization threshold contains $N\sim 2\times 10^4$ principal components.

III. RECOMBINATION

For low-energy electrons the contribution of the autoionizing states (resonances) to the recombination cross section is given by (see, e.g., Ref. [27])

$$\sigma_r=\frac{\pi}{k^2}\sum_\nu\frac{2J+1}{2(2J_i+1)}\frac{\Gamma_\nu^{(r)}\Gamma_\nu^{(a)}}{(\varepsilon-\varepsilon_\nu)^2+\Gamma_\nu^2/4}, \tag{4}$$

where $\varepsilon = k^2/2$ is the electron energy, J_i is the angular momentum of the initial (ground) target state, J are the angular momenta of the resonances, $\varepsilon_\nu = E_\nu - I$ is the position of the νth resonance relative to the ionization threshold of the compound (final-state) ion, and $\Gamma_\nu^{(a)}$, $\Gamma_\nu^{(r)}$, and $\Gamma_\nu = \Gamma_\nu^{(r)} + \Gamma_\nu^{(a)}$ are its autoionization, radiative, and total widths, respectively [28]. When the resonance spectrum is dense, σ_r can be averaged over an energy interval $\Delta\varepsilon$ which contains many resonances, $D \ll \Delta\varepsilon \ll \varepsilon$, yielding

$$\overline{\sigma}_r = \frac{2\pi^2}{k^2} \sum_{J^\pi} \frac{2J+1}{2(2J_i+1)D} \left\langle \frac{\Gamma_\nu^{(r)}\Gamma_\nu^{(a)}}{\Gamma_\nu^{(r)}+\Gamma_\nu^{(a)}} \right\rangle, \tag{5}$$

where $\langle \cdots \rangle$ means averaging. If the fluorescence yield $\omega_f \equiv \Gamma_\nu^{(r)}/(\Gamma_\nu^{(r)}+\Gamma_\nu^{(a)})$ fluctuates weakly from resonance to resonance (see below), one can write $\overline{\sigma}_r = \overline{\sigma}_c \omega_f$, where

$$\overline{\sigma}_c = \frac{\pi^2}{k^2} \sum_{J^\pi} \frac{(2J+1)\Gamma^{(a)}}{(2J_i+1)D} \tag{6}$$

is the energy-averaged capture cross section, and $\Gamma^{(a)}$ is the average autoionization width.

Unlike complex multiply excited states Ψ_ν, the initial state of the recombination process is simple. It describes an electron with the energy ε incident on the ground state Φ_i of the target, which is often dominated by one configuration. For example, in the ion of interest it is $Au^{25+} 4f^8$, $J_i = 6$ [19]. The autoionization width is given by perturbation theory as

$$\begin{aligned}\Gamma_\nu^{(a)} &= 2\pi |\langle \Psi_\nu | \hat{V} | \Phi_i ; \varepsilon \rangle|^2 \\ &= 2\pi \sum_{k,k'} C_k^{(\nu)*} C_{k'}^{(\nu)} \langle \Phi_i ; \varepsilon | \hat{V} | \Phi_{k'} \rangle \langle \Phi_k | \hat{V} | \Phi_i ; \varepsilon \rangle,\end{aligned} \tag{7}$$

where $\hat{V}$ is the electron Coulomb interaction, and the continuum states ε are normalized to unit energy interval. Averaging $\Gamma_\nu^{(a)}$ over the chaotic states ν with $E_\nu \approx I + \varepsilon$, we make use of the fact that their components are random and uncorrelated, which leads to

$$\Gamma^{(a)} = 2\pi \sum_k \overline{|C_k^{(\nu)}|^2} |\langle \Phi_k | \hat{V} | \Phi_i ; \varepsilon \rangle|^2. \tag{8}$$

Being a two-body operator, $\hat{V}$ can move only two electrons at a time. Therefore, a nonzero contribution to $\Gamma^{(a)}$ is given by the basis states that differ from the initial state $|\Phi_i ; \varepsilon\rangle$ by the positions of two electrons, and in Eq. (8) we need to sum over *doubly excited* basis states Φ_d only. With the help of Eq. (3) the capture cross section (6) becomes

$$\overline{\sigma}_c = \frac{\pi}{k^2} \sum_d \frac{2J+1}{2(2J_i+1)} \frac{\Gamma_{\rm spr} 2\pi |\langle \Phi_d | \hat{V} | \Phi_i ; \varepsilon \rangle|^2}{(E_d - I - \varepsilon)^2 + \Gamma_{\rm spr}^2/4}. \tag{9}$$

This form makes it clear [cf. Eq. (4)] that the two-electron excitations Φ_d play the role of *doorway states* for the electron capture process. Since these states are not the eigenstates of the system they have a finite energy width $\Gamma_{\rm spr}$.

The wave function of a doorway state can be constructed using the creation-annihilation operators $|\Phi_d\rangle = a_\alpha^\dagger a_\beta^\dagger a_\gamma |\Phi_i\rangle$, where $\alpha \equiv n_\alpha l_\alpha j_\alpha m_\alpha$ and $\beta \equiv n_\beta l_\beta j_\beta m_\beta$ are excited single-electron states, and $\gamma \equiv n_\gamma l_\gamma j_\gamma m_\gamma$ corresponds to a hole in the target ground state. (Note that we are using relativistic Dirac-Fock orbitals $nljm$.) Of course, to form doorway states with a given J the angular momenta of the electrons and ionic residue must be coupled into the total angular momentum J. However, the $2J+1$ factor and summation over J implied in Eq. (9) account for all possible couplings, and we can simply sum over the single-electron excited states α, β and hole states γ, as well as the partial waves lj of the continuous-spectrum electron ε. As a result, we have

$$\begin{aligned}\overline{\sigma}_c = \frac{\pi^2}{k^2} \sum_{\alpha\beta\gamma,lj} & \frac{\Gamma_{\rm spr}}{(\varepsilon - \varepsilon_\alpha - \varepsilon_\beta + \varepsilon_\gamma)^2 + \Gamma_{\rm spr}^2/4} \\ & \times \sum_\lambda \frac{\langle \alpha,\beta \| V_\lambda \| \gamma, \varepsilon lj \rangle}{2\lambda+1} \Bigg[\langle \alpha,\beta \| V_\lambda \| \gamma, \varepsilon lj \rangle \\ & - (2\lambda+1) \sum_{\lambda'} (-1)^{\lambda+\lambda'+1} \begin{Bmatrix} \lambda & j_\alpha & j \\ \lambda' & j_\beta & j_\gamma \end{Bmatrix} \\ & \times \langle \alpha,\beta \| V_{\lambda'} \| \varepsilon lj, \gamma \rangle \Bigg],\end{aligned} \tag{10}$$

where ε_α, ε_β, and ε_γ are the orbital energies, the two terms in square brackets represent the direct and exchange contributions, and $\langle \alpha,\beta \| V_\lambda \| \gamma, \varepsilon lj \rangle$ is the reduced Coulomb matrix element:

$$\begin{aligned}&\langle \alpha,\beta \| V_\lambda \| \gamma, \delta \rangle \\ &= \sqrt{(2j_\alpha+1)(2j_\beta+1)(2j_\gamma+1)(2j_\delta+1)} \\ &\quad \times \xi(l_\alpha + l_\delta + \lambda) \xi(l_\beta + l_\gamma + \lambda) \begin{pmatrix} \lambda & j_\alpha & j_\delta \\ 0 & -\frac{1}{2} & \frac{1}{2} \end{pmatrix} \\ &\quad \times \begin{pmatrix} \lambda & j_\beta & j_\gamma \\ 0 & -\frac{1}{2} & \frac{1}{2} \end{pmatrix} R_\lambda(\alpha,\beta;\gamma,\delta).\end{aligned} \tag{11}$$

Here $\xi(L) = [1 + (-1)^L]/2$ is 0 (1) for an odd (even) L, and

$$\begin{aligned}R_\lambda(\alpha,\beta;\gamma,\delta) = \int\int \frac{r_<^\lambda}{r_>^{\lambda+1}} & [f_\alpha(r) f_\delta(r) + g_\alpha(r) g_\delta(r)] \\ & \times [f_\beta(r') f_\gamma(r') + g_\beta(r') g_\gamma(r')] dr dr'\end{aligned} \tag{12}$$

is the radial Coulomb integral, f and g being the upper and lower components of the relativistic orbital spinors.

Equation (10) is directly applicable to targets with closed-shell ground states. If the target ground state contains partially occupied orbitals, a factor

$$\frac{n_\gamma}{2j_\gamma+1}\left(1-\frac{n_\alpha}{2j_\alpha+1}\right)\left(1-\frac{n_\beta}{2j_\beta+1}\right), \tag{13}$$

where n_α, n_β, and n_γ are the orbital occupation numbers in the ground state Φ_i, must be introduced on the right-hand side of Eq. (10). Steps similar to those that lead to Eq. (10) were used to obtain mean-squared matrix elements of operators between chaotic many-body states [25,29].

The chaotic nature of the multiply excited states Ψ_ν can also be employed to estimate their radiative widths $\Gamma_\nu^{(r)}$. Electron-photon interaction is described by a single-particle dipole operator $\hat{d}$. Any excited electron in Ψ_ν may emit a photon, thus leading to radiative stabilization of this state. The total photoemission rate $\Gamma_\nu^{(r)}$ can be estimated as a weighted sum of the single-particle rates,

$$\Gamma_\nu^{(r)} \simeq \sum_{\alpha,\beta} \frac{4\omega_{\beta\alpha}^3}{3c^3}|\langle\alpha\|\hat{d}\|\beta\rangle|^2 \times\left\langle \frac{n_\beta}{2j_\beta+1}\left(1-\frac{n_\alpha}{2j_\alpha+1}\right)\right\rangle_\nu, \tag{14}$$

where $\omega_{\beta\alpha}=\varepsilon_\beta-\varepsilon_\alpha>0$, $\langle\alpha\|\hat{d}\|\beta\rangle$ is the reduced dipole operator between the orbitals α and β, and $\langle\cdots\rangle_\nu$ is the mean occupation number factor. Since Ψ_ν have large numbers of principal components N, their radiative widths display small $1/\sqrt{N}$ fluctuations. This can also be seen if one recalls that a chaotic multiply excited state is coupled by photoemission to many lower-lying states, and the total radiative width is the sum of a large number of (strongly fluctuating) partial widths. A similar effect is known in compound nucleus resonances in low-energy neutron scattering [20].

There is a certain similarity between Eqs. (10) and (14) and those for autoionization and radiative rates obtained in a so-called configuration-average approximation [30]. In both cases the answers involve squares or products of two-body Coulomb matrix elements [see the direct and exchange terms in Eq. (10)], or single-particle dipole amplitudes [Eq. (14)]. However, there are a number of important differences between the present results and the configuration-average approximation. The latter considers dielectronic recombination and introduces averaging over configurations as a means of simplifying the calculation. The DR cross section is averaged over an arbitrary energy interval $\Delta\varepsilon$, and only the configurations within this energy range contribute to the average. Effects of configuration mixing as well as level mixing within a configuration are neglected.

On the other hand, our method applies to complex (open-shell) systems with an extreme degree of configuration mixing. The dielectronic states involved in Eq. (10) are only doorways to the more complicated multiply excited resonance states that mediate recombination. The averaging performed in deriving Eqs. (5) or (10) is done over an energy interval $\Delta\varepsilon$ which contains several resonances. It is small owing to very small spacings between the resonances, and does not appear explicitly in the final formula. In the regime of strong configuration mixing characterized by $\Gamma_{\rm spr}$, the weighted averaging over a number of two-electron doorway configurations expressed by Eq. (10) does take place naturally within the system. It is not enforced as a calculation tool by the researcher.

It is important to compare the radiative and autoionization widths of chaotic multiply excited states. Equation (14) shows that $\Gamma^{(r)}$ is comparable to the single-particle radiative widths. On the other hand, the autoionization width $\Gamma^{(a)}$, Eq. (8), is suppressed by a factor $|C_k^{(\nu)}|^2\sim N^{-1}$ relative to that of a typical dielectronic resonance. A comparison of Eqs. (6) and (9) also shows that $\Gamma^{(a)}$ is suppressed as $D/\Gamma_{\rm spr}$. Therefore, in systems with dense spectra of chaotic multiply excited states the autoionization widths are small. Physically this happens because the coupling strength of a two-electron doorway state to the continuum is shared between many complicated multiply excited eigenstates. As a result, the radiative width may dominate the total width of the resonances, $\Gamma^{(r)}\gg\Gamma^{(a)}$, making their fluorescence yield close to unity. Our numerical results for the recombination of Au^{25+} presented in Sec. IV, confirm this scenario.

The resonance recombination cross section should be compared with the direct radiative recombination cross section

$$\sigma_d=\frac{32\pi}{3\sqrt{3}c^3}\frac{Z_i^2}{k^2}\ln\left(\frac{Z_i}{n_0 k}\right) \tag{15}$$

obtained from the Kramers formula by summing over the principal quantum number of the final state [19]. Here Z_i is the ionic charge ($Z_i=25$ for Au^{25+}), and n_0 is the principal quantum number of the lowest unoccupied ionic orbital ($n_0=5$). Note that the direct and energy-averaged resonance recombination cross sections of Eqs. (15) and (5) have similar energy dependences. Therefore, for the purpose of comparing with experiment we can evaluate the cross sections at one low energy, say $\varepsilon=0.5$ eV. This energy is much greater than the thermal energy spread of the electron beam [2] and the cross sections can be compared directly to the experiment [1].

IV. NUMERICAL RESULTS

Numerical calculations of the cross section from Eqs. (10) and (13) involve summation over the orbitals shown in Fig. 1 and electron partial waves up to $h_{11/2}$. Here we also use the fact that the Au^{25+} ground state is to a good approximation described by the $4f^8$ configuration. The latter is true because this configuration is separated from any excited state configurations by an energy gap greater than the spread of the $4f^8$ configuration itself. This ensures that admixtures of higher-lying configurations to the ground state are small [32].

As a result, we obtain the capture cross section $\overline{\sigma_c}=23\times10^{-16}$ cm^2 at $\varepsilon=0.5$ eV. A comparison with Eq. (6) shows that the sum, which contains the autoionization width, is

$$\overline{\sigma_c}\frac{k^2}{\pi^2}=\sum_{J^\pi}\frac{(2J+1)\Gamma^{(a)}}{(2J_i+1)D}=0.305. \tag{16}$$

It is worth mentioning that direct terms in the sum (10) dominate strongly over the exchange terms, their respective contributions to Eq. (16) being 0.3185 and -0.0138. Combining the result (16) with $D=3\times10^{-5}$ a.u. and taking into account that about ten different J and two parities contribute to the sum, we obtain $\Gamma^{(a)}\sim5\times10^{-7}$ a.u. On the other hand, a numerical calculation of Eq. (14) gives $\Gamma^{(r)}=3\times10^{-5}$ a.u. Therefore, $\Gamma^{(r)}\gg\Gamma^{(a)}$ and $\omega_f\approx1$. Hence, the resonance recombination cross section is essentially equal to the capture cross section: $\overline{\sigma_r}\approx23\times10^{-16}$ cm^2. This value is in good agreement with the experimental $\sigma^{(\mathrm{expt})}=27\times10^{-16}$ cm^2 [1], and exceeds the direct recombination cross section (15), $\sigma_d=0.12\times10^{-16}$ cm^2, by a factor of 200.

Note that the relation between the radiative and autoionization widths $\Gamma^{(r)}\gg\Gamma^{(a)}$ established in the present calculation is opposite to the assumption we made in Ref. [19]. This is an important point and we shall discuss it before taking a closer look at our numerical results. It is often assumed that for autoionizing states involving electron orbitals with low principal quantum numbers the autoionization rate is greater than the radiative rate. This understanding is based on the fact that autoionization is mediated by the "strong" Coulomb interaction between the electrons, while the probability to emit a photon depends on the "weak" electromagnetic interaction, and is inversely proportional to c^3, where the speed of light is a large number, $c\approx137$ in atomic units [31]. In Au^{24+} and similar complex open-shell systems the autoionizing states are formed by strongly mixed multiply excited electron configurations, most of which do not have direct coupling to the electron-target continuum. As a result, their autoionization widths are suppressed compared to those of simple dielectronic resonances ($\Gamma^{(a)}\propto N^{-1}\propto D$, see Sec. III), while their radiative widths retain the magnitude characteristic of the single-particle transitions involved, Eq. (14). This leads to large fluorescence yields and, as in the case of Au^{24+}, is important for understanding high resonance recombination rates.

Table I lists the most important dielectronic doorway contributions to the dimensionless sum in Eq. (10), which also determines the ratio of the autoionization width to the spacing between the resonances, Eq. (16). In total they account for about two-thirds of the total cross section. Although these transitions have been selected according to the size of their contributions to Eq. (16), their energies are close to the threshold, as seen in the last column in Table I. Indeed, the spreading of configurations discussed in Sec. II allows configurations near the threshold, $|\Delta E|\lesssim\Gamma_{\mathrm{spr}}$, to contribute. On the other hand, the contribution of configurations lying far away from threshold, $|\Delta E|\gg\Gamma_{\mathrm{spr}}$, is suppressed.

Apart from the $1/k^2$ factor, the scale of the energy dependence of the recombination cross section (10) is determined by Γ_{spr}. Therefore, for electron energies $\varepsilon\sim1$ eV $\ll\Gamma_{\mathrm{spr}}$ the dimensionless sum (16) can be regarded as constant. This is why the energy dependence of the resonance and direct radiative recombination cross sections are similar at low energies, apart from a weak logarithmic factor in Eq. (15). It is easy to make a more detailed comparison with the experimental data of Ref. [1] by calculating thermally averaged recombination rates:

TABLE I. Electron orbitals that give the leading contributions to the low-energy electron recombination on Au^{25+}.

Orbitals[a]					
α	β	γ	εlj	Direct contribution[b]	ΔE[c] (a.u.)
$7s_{1/2}$	$4f_{7/2}$	$4d_{5/2}$	$p_{1/2}$	0.0094	0.062
$7s_{1/2}$	$4f_{7/2}$	$4d_{5/2}$	$p_{3/2}$	0.0257	0.062
$6p_{3/2}$	$5f_{5/2}$	$4f_{5/2}$	$p_{3/2}$	0.0142	-0.202
$7p_{1/2}$	$4f_{7/2}$	$4d_{5/2}$	$d_{3/2}$	0.0061	0.539
$5d_{3/2}$	$5d_{5/2}$	$4d_{5/2}$	$d_{3/2}$	0.0053	0.740
$6f_{5/2}$	$4f_{7/2}$	$4d_{5/2}$	$d_{3/2}$	0.0052	-0.330
$5d_{5/2}$	$6f_{5/2}$	$4f_{5/2}$	$d_{5/2}$	0.0068	-0.364
$6f_{7/2}$	$4f_{7/2}$	$4d_{5/2}$	$d_{5/2}$	0.0091	-0.303
$5f_{5/2}$	$5g_{9/2}$	$4f_{7/2}$	$g_{7/2}$	0.0056	0.247
$5f_{5/2}$	$5g_{7/2}$	$4f_{5/2}$	$g_{7/2}$	0.0085	0.423
$5g_{7/2}$	$5f_{7/2}$	$4f_{7/2}$	$g_{7/2}$	0.0091	0.297
$5g_{7/2}$	$5f_{5/2}$	$4f_{5/2}$	$g_{7/2}$	0.0163	0.423
$5f_{7/2}$	$5g_{9/2}$	$4f_{7/2}$	$g_{9/2}$	0.0062	0.299
$5f_{7/2}$	$5g_{7/2}$	$4f_{5/2}$	$g_{9/2}$	0.0097	0.474
$5g_{9/2}$	$5f_{7/2}$	$4f_{7/2}$	$g_{9/2}$	0.0112	0.299
$5g_{9/2}$	$5f_{5/2}$	$4f_{5/2}$	$g_{9/2}$	0.0201	0.424
$6g_{7/2}$	$4f_{7/2}$	$4d_{5/2}$	$h_{9/2}$	0.0144	1.060
$6g_{9/2}$	$4f_{7/2}$	$4d_{5/2}$	$h_{11/2}$	0.0176	1.062

[a] α and β are the excited electron orbitals, and γ is the ground-state hole of the dielectronic doorway state; εlj is the partial wave of the incident electron.

[b] Direct term contributions to the dimensionless sum in Eq. (10), $\overline{\sigma_c}k^2/\pi^2$, as in Eq. (16), with magnitudes greater than 5×10^{-3}.

[c] $\Delta E=\varepsilon_\alpha+\varepsilon_\beta-\varepsilon_\gamma$ is the mean-field energy of the doorway state relative to the threshold.

$$\alpha(v_{\mathrm{rel}})=\int v\,\sigma(v)\exp\left(-\frac{v_\perp^2}{2k_BT_\perp}\right)\exp\left(-\frac{(v_\parallel-v_{\mathrm{rel}})^2}{2k_BT_\parallel}\right)\times\frac{2\pi v_\perp dv_\perp dv_\parallel}{2\pi k_BT_\perp\sqrt{2\pi k_BT_\parallel}},\tag{17}$$

where v_{rel} is the average longitudinal velocity of the electron beam relative to the ions, $v=(v_\perp^2+v_\parallel^2)^{1/2}=k$ in atomic units, $v_\perp$ and $v_\parallel$ are the transversal and longitudinal velocity components, respectively, $T_\perp$ and $T_\parallel$ are the corresponding temperatures of the beam, and k_B is Boltzmann's constant.

According to Ref. [1], the two temperatures of the beam are very different, $k_BT_\parallel=1$ meV and $k_BT_\perp=0.1$ eV. This allows one to do the integral in Eq. (17) analytically for the cross section of the form $\sigma(v)=A/v^2$, as that of the resonance recombination, to obtain

$$\alpha(v_{\mathrm{rel}})=A\sqrt{\frac{\pi}{2k_BT_\perp}}\exp\left(\frac{v_{\mathrm{rel}}^2}{2k_BT_\perp}\right)\times\left[1-\Phi\left(\sqrt{\frac{v_{\mathrm{rel}}^2}{2k_BT_\perp}}\right)\right],\tag{18}$$

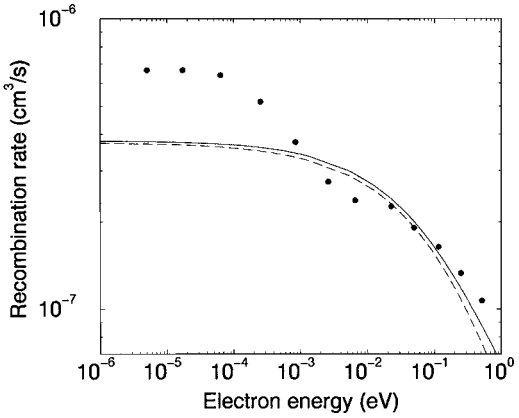

FIG. 2. Electron recombination rate on Au^{25+}. The solid line is the thermally-averaged resonance recombination rate as given by Eq. (18) with $A=0.305\times\pi^2$ a.u. [cf. Eq. (16)] and $T_\perp=0.1$ eV. The dashed line is the velocity-averaged radiative recombination rate obtained using Eq. (15) and multiplied by 190. Solid circles represent the experimental results of Ref. [1].

where Φ is the error function [$\Phi(0)=0$, and $\Phi(x)\simeq 1-e^{-x^2}/(x\sqrt{\pi})$ for $x\gg 1$]. In particular, for $v_{\rm rel}^2\gg k_B T_\perp$, Eq. (18) gives $\alpha(v_{\rm rel})\simeq A/v_{\rm rel}$. The thermal averaging of the direct radiative recombination cross section (15) can be done numerically. The corresponding rates are shown in Fig. 2 together with the experimental results. Rather than showing the actual experimental data, which contain hundreds of points with error bars, we have chosen a relatively small set of points that traces out the overall energy dependence of the rate, free from uncertainties and "noise."

As expected, the energy dependences of the resonance and direct recombination rates are very close, although the latter is about 200 times smaller. There is a good overall agreement between the resonance rate and experimental data at electron energies above 10^{-2} eV. As explained in [3], the enhanced experimental rates at low electron energies are unlikely to have anything to do with the electronic structure of the target ion. Moreover, experiments with bare ions show that this type of enhancement is limited to the meV and sub-meV electron energy range, and does not have a long high-energy "tail," which would enhance the rate at $\varepsilon\sim 0.1$ eV and above.

V. SUMMARY AND OUTLOOK

In summary, we have shown that a dense spectrum of chaotic multiply excited states can play a major role in the dynamics of electron recombination with many-electron multicharged ions, and possibly other processes, e.g., charge transfer in collisions between multiply charged ions and neutral atoms. Based on the chaotic nature of these states, we have developed a statistical theory which enables one to calculate energy-averaged cross sections for processes that go via such resonances. Applied to the recombination of Au^{25+}, the theory shows that the contribution of resonances exceeds that of direct radiative recombination 200 times, which explains the recent experimental findings [1].

Although electron recombination with Au^{25+} seems an exotic example, the occurrence of dense spectra of multiply excited strongly mixed states ("many-body quantum chaos") is a rather common phenomenon in atoms and molecules (see, e.g., [33,34]), as well as in nuclei [24], and, possibly, mesoscopic solid-state systems such as quantum dots [35]. Therefore, we are dealing with a general phenomenon. The main theoretical problem here is to describe such states and develop a statistical theory that would allow one to calculate their properties and obtain observable quantities, e.g., cross sections, in a situation where it is impracticable and often impossible to perform exact diagonalization of a huge Hamiltonian matrix. Over the past few years considerable progress has been made toward such a theory [24,25,29,36]. However, more work is needed on both the theoretical and experimental sides.

From this point of view complex multicharged ions can be regarded as laboratories for studying many-body quantum chaos, and the process of low-energy electron recombination could be a very useful tool for such studies.

ACKNOWLEDGMENT

We thank Professor A. Müller for providing experimental data in numerical form.

[1] A. Hoffknecht *et al.*, J. Phys. B **31**, 2415 (1998).
[2] The experimental energy resolution in Ref. [1] was limited by the transversal temperature of the electron beam $kT_\perp=0.1$ eV.
[3] Below 1 meV the measured rate showed an additional enhancement. This enhancement, which depends on the electron beam temperatures $T_\parallel$ and $T_\perp$ and the magnetic field, is the subject of ongoing research, see, e. g., G. Gwinner *et al.*, Phys. Rev. Lett. **84**, 4822 (2000). It has been observed even for bare ions; H. Gao *et al.*, J. Phys. B **30**, L499 (1997); O. Uwira *et al.*, Hyperfine Interact. **108**, 167 (1997). We do not consider it here.
[4] H.S.W. Massey and D.R. Bates, Rep. Prog. Phys. **9**, 62 (1943).
[5] A. Burgess, Astrophys. J. **139**, 776 (1964).
[6] *Recombination of Atomic Ions*, Vol. 296 of *NATO Advanced Study Institute, Series B: Physics*, edited by W. G. Graham, W. Fritsch, Y. Hahn, and J. A. Tanis (Plenum Press, New York, 1992).
[7] L.H. Andersen, P. Hvelplund, H. Knudsen, and P. Kvistgaard, Phys. Rev. Lett. **62**, 2656 (1989).
[8] G. Kilgus *et al.*, Phys. Rev. Lett. **64**, 737 (1990).
[9] S. Schennach *et al.*, Z. Phys. D: At., Mol. Clusters **30**, 291 (1994).
[10] H. Gao *et al.*, Phys. Rev. Lett. **75**, 4381 (1995).
[11] R. Shuch *et al.*, Hyperfine Interact. **99**, 317 (1996).
[12] O. Uwira *et al.*, Hyperfine Interact. **99**, 295 (1996).
[13] O. Uwira *et al.*, Hyperfine Interact. **108**, 149 (1997).
[14] W. Zong *et al.*, Phys. Rev. A **56**, 386 (1997).
[15] S. Mannervik *et al.*, Phys. Rev. Lett. **81**, 313 (1998).
[16] D.R. DeWitt *et al.*, Phys. Rev. A **50**, 1257 (1994); J. Phys. B **28**, L147 (1995).

[17] D.R. DeWitt *et al.*, Phys. Rev. A **53**, 2327 (1996).
[18] D.M. Mitnik *et al.*, Phys. Rev. A **57**, 4365 (1998).
[19] G.F. Gribakin, A.A. Gribakina, and V.V. Flambaum, Aust. J. Phys. **52**, 443 (1999); see also e-print physics/9811010.
[20] A. Bohr and B. Mottelson, *Nuclear Structure* (Benjamin, New York, 1969), Vol. 1.
[21] This fit is valid for $E>1$ a.u. In the Fermi-gas model a is related to the single-particle level density at the Fermi level $g(\varepsilon_F)=3a^2/2\pi^2$. The fitted value $a=3.35$ gives $g(\varepsilon_F)=1.7$ a. u., in agreement with the orbital spectrum in Fig. 1.
[22] J.N. Ginocchio, Phys. Rev. Lett. **31**, 1260 (1973); J. Bauche and C. Bauche-Arnoult, J. Phys. B **20**, 1659 (1987).
[23] The level density for each configuration can be evaluated more accurately by taking its higher moments into account. See, e.g., R. Karazija, *Sums of Atomic Quantities and Mean Characteristics of Spectra* (Mokslas, Vilnius, 1991) or J. Bauche, C. Bauche-Arnoult, and M. Klapisch, Adv. At. Mol. Phys. **23**, 131 (1988).
[24] V. Zelevinsky, B.A. Brown, M. Frazier, and M. Horoi, Phys. Rep. **276**, 85 (1996).
[25] V.V. Flambaum, A.A. Gribakina, G.F. Gribakin, and M.G. Kozlov, Phys. Rev. A **50**, 267 (1994); V.V. Flambaum, A.A. Gribakina, and G.F. Gribakin, *ibid.* **54**, 2066 (1996); **58**, 230 (1998).
[26] We should point out that in Ref. [19] these two configurations were identified incorrectly due to a misprint.
[27] L. D. Landau and E. M. Lifshitz, *Quantum Mechanics*, 3rd ed. (Pergamon, Oxford, 1977).
[28] Here we assume that the electron energy is below the target excitation threshold.
[29] V.V. Flambaum and O.K. Vorov, Phys. Rev. Lett. **70**, 4051 (1993).
[30] D.C. Griffin, M.S. Pindzola, and C. Bottcher, Phys. Rev. A **31**, 568 (1985).
[31] For autoionizing states involving Rydberg states with large principal quantum numbers the Coulomb interaction is weakened due to large electron orbital radii. In this case the radiative rate may become dominant over the autoionization rate. This is also true for highly charged ions, where radiative transitions are enhanced by the large ω^3 factor.
[32] It is typical for many-body Fermi systems that the regime of strong mixing and, ultimately, quantum chaos is found at higher excitation energies, whereas the ground and low-lying excited states remain ''regular'' and simple. See, e.g., P. Jacquod and D.L. Shepelyansky, Phys. Rev. Lett. **79**, 1837 (1997); B.L. Altshuler, Y. Gefen, A. Kamenev, and L.S. Levitov, *ibid.* **78**, 2803 (1997); or Ref. [24] where the onset of quantum chaos in nuclei is considered.
[33] J.P. Connerade, M.A. Baig, and M. Sweeney, J. Phys. B **23**, 713 (1990); J.P. Connerade, I.P. Grant, P. Marketos, and J. Oberdisse, *ibid.* **28**, 2539 (1995); J.P. Connerade, *ibid.* **30**, L31 (1997).
[34] T. Zimmermann, H. Köppel, L.S. Cederbaum, G. Persch, and W. Demtröder, Phys. Rev. Lett. **61**, 3 (1988).
[35] A.J. Fendrik, M.J. Sanchez, and P.I. Tamborenea, Phys. Rev. B **63**, 115313 (2001).
[36] V.V. Flambaum and F.M. Izrailev, Phys. Rev. E **61**, 2539 (1998); V.V. Flambaum and G.F. Gribakin, Philos. Mag. B **80**, 2143 (2000), and references therein.